Available online at www.sciencedirect.com
SCIENCE DIRECT®
International Journal of Heat and Mass Transfer 48 (2005) 3722–3735
International Journal of HEAT and MASS TRANSFER
www.elsevier.com/locate/ijhmt

Heat and mass fluxes across density interfaces in a grid-generated turbulence

Y. Zellouf, P. Dupont, H. Peerhossaini *

Thermofluids, Complex Flows and Energy Research Group, Laboratoire de Thermocinétique CNRS UMR 6607, Ecole Polytechnique de l'Université de Nantes, rue Christian Pauc, B.P. 50609, Nantes Cedex 3, 44306, France

Received 1 October 2004; received in revised form 18 March 2005
Available online 26 May 2005

Abstract

We present heat and salt fluxes measurements across a single density-stratified interface in a grids-generated turbulence system. The turbulent field is measured in a homogeneous medium (water) by Particle Image Velocimetry (PIV). Stratifications have been followed in time by recording the vertical temperature and density profiles. Measured buoyancy heat and mass fluxes show two different behaviors similar to that in double diffusive convection systems. This was also highlighted by measurement of entrainment rate near the interface, which showed that entrainment depends on the diffusivity for high Richardson number *Ri*. For low *Ri*, molecular diffusion has less effect on the transport process than turbulent mixing.

Keywords: Heat and mass transfer; Stratified flows; Density interface; Grid turbulence; PIV measurements

1. Introduction

Mixing across a density interface in stratified flows has been investigated in natural as well as industrial situations because of its importance in the vertical transport of different species across such interfaces [1–4]. Huppert and Turner [5] reviewed the many geophysical and industrial applications of these flows, commonly called *double-diffusive convection*. Their fundamental characteristic is the formation of a system of two horizontal homogeneous layers separated by sharp diffusive interfaces of linear density. In most such situations, the characteristic length and velocity scales are large, ensuring a turbulent flow everywhere that maintains well-mixed layers, sharpens the interface, and produces mixing across the density interface. The vertical transport of different species between the turbulent mixed layers is thus influenced by mixing across the density interface.

The ways in which turbulence is generated in the laboratory vary from one study to another, often because of the specific phenomena studied. In general, two kinds of experiments are used: turbulence generated by mean shear flow and turbulence generated by grid oscillation with zero mean shear. According to Turner [6], the vertically oscillating grid is the more appropriate way to generate turbulence: one or a pair of grids is oscillated vertically in an initially stably density gradient or in

* Corresponding author. Tel.: +33 2 40 68 31 39; fax: +33 2 40 68 31 41.
E-mail address: hassan.peerhossaini@polytech.univ-nantes.fr (H. Peerhossaini).

0017-9310/$ - see front matter © 2005 Elsevier Ltd. All rights reserved.
doi:10.1016/j.ijheatmasstransfer.2005.03.022

Nomenclature

A_{int}	interfacial area (m^2)
A_{losses}	surface heat losses (m^2)
c_p	constant-pressure specific heat ($J\,kg^{-1}\,K^{-1}$)
f	grid oscillation frequency (Hz)
F_S	interfacial flux of salt ($kg\,m^{-2}\,s^{-1}$)
F_T	interfacial flux of heat ($W\,m^{-2}$)
F_{SP}	salt flux across a solid plate ($kg\,m^{-2}\,s^{-1}$)
F_{TP}	heat flux across a heated solid plate ($W\,m^{-2}$)
g	gravitational acceleration ($m\,s^{-2}$)
h_l	lower layer depth (m)
h_u	upper layer depth (m)
h_{int}	interface thickness (m)
H	total stratification depth ($=h_l + h_{int} + h_u$) (m)
L_{int}	size of interrogation area (m)
l'	horizontal turbulent length scale (m)
M	grid mesh size (m)
Nu	Nusselt number
Pe	Peclet number
S	salt concentration (g of salt per 100 g solution) (%)
s	grid oscillation stroke (m)
Sc	Schmidt number
Sh	Sherwood number
T	temperature (°C, K)
t	time (s)
R	spatial autocorrelation function
Ra	Rayleigh number
Re	Reynolds number
Ri	Richardson number
R_ρ	interfacial stability ratio
U	horizontal mean velocity ($m\,s^{-1}$)
u_e	entrainment velocity ($m\,s^{-1}$)
u	fluctuating horizontal velocity ($m\,s^{-1}$)
u'	horizontal rms velocity ($m\,s^{-1}$)
V	vertical mean velocity ($m\,s^{-1}$)
v	fluctuating vertical velocity ($m\,s^{-1}$)
v'	vertical rms velocity ($m\,s^{-1}$)
z_g	distance from grids (m)
$\Delta\rho$	density difference between mixed layers ($kg\,m^{-3}$, $g\,cm^{-3}$)
ΔS	concentration difference between mixed layers (%)
ΔT	temperature difference between mixed layers (°C, K)

Greek symbols

α	thermal expansion coefficient $= -\frac{1}{\rho}(\frac{\partial\rho}{\partial T})_S$ (K^{-1})
β	mass expansion coefficient $= -\frac{1}{\rho}(\frac{\partial\rho}{\partial S})_T$
φ_{losses}	heat losses (W)
k_T	thermal molecular diffusivity ($m^2\,s^{-1}$)
k_S	salt diffusivity ($m^2\,s^{-1}$)
λ_{ins}	insulation thermal conductivity ($W\,m^{-1}\,K^{-1}$)
ν	kinematic viscosity ($m^2\,s^{-1}$)
ρ	density ($kg\,m^{-3}$, $g\,cm^{-3}$)
ρ_0	density reference of the lower layer at T_0, S_0 ($kg\,m^{-3}$, $g\,cm^{-3}$)
$\langle\,\rangle_i$	average in the x-direction

initially homogeneous layers at some distance from a density interface [1,7–9].

Turbulence generated by grid oscillation is characterized by experimental parameters that enter directly into its generation. Thompson and Turner [2] measured the properties of this turbulence in a homogeneous fluid using a hot film. They showed that their statistical quantities, defined as the horizontal rms velocity u' and the turbulent integral length scale l', depend strongly on the overall experimental parameters: the oscillation frequency f, the stroke s of the grid, the distance z_g away from the grid and the shape of the grid. They found that, for a square-barred grid with $s = 10$ mm, u' depends linearly on the stirring frequency f and decays as the -1.5 power with vertical distance z_g from the centre of the grid midplane. They also found that the integral length scale l' increases linearly with distance z_g from the grid. Hopfinger and Tolly [10], defining a virtual origin z'_g at which $l' = 0$, proposed an empirical turbulence decay law of the form

$$\frac{u'}{f_s} = C_1\left(\frac{s}{M}\right)^{0.5}\left(\frac{z'}{M}\right)^{-1} \tag{1}$$

for $M/d = 5$, where M is the grid mesh size and d is the bar size. The experimental constant was equal to 0.25 for a stroke s ranging from 40 to 90 mm. Ura et al. [11] give the same relationship with $C_1 = 0.19$ in the range $z_g/M \leqslant 5$. This form of the equation is widely used because of its simplicity.

Turner [12] measured the mixing rate across a density interface between two layers of liquid where the density difference across the interface is produced by heat or salt and the stirring is generated in one or both layers. His results suggest that the mixing rate across a density interface depends on the competition between inertial forces due to turbulence and the potential energy of the stratification defined through the overall Richardson number

$$Ri = g\frac{\Delta\rho}{\rho}\frac{l'}{u'^2} \tag{2}$$

where g is the gravitational acceleration, $\Delta\rho$ is the interfacial density step and ρ is the mixed layer density. He proposed an empirical correlation for the mixing rate E of the form

$$E = \frac{u_e}{u'} \propto Ri^{-n} \tag{3}$$

where the entrainment velocity is defined in the case of one layer as the mean rate of advance of the interface

$$u_e = \frac{dh}{dt} \tag{4}$$

where h is the layer depth. On the other hand, when both layers are stirred at the same rate, the interface remains sharp and central. Turner [12] introduced an indirect measure of u_e (in one direction) based on the rate of change of properties in the layers:

$$u_e = \frac{h}{S_l - S_u}\frac{dS_u}{dt} \tag{5}$$

$$u_e = \frac{h}{T_u - T_l}\frac{dT_l}{dt} \tag{6}$$

where dS_u/dt is the rate of change of the concentration in the upper layer in the salt-stratification case and dT_l/dt is the rate of change of temperature in the lower layer in the temperature-stratification case. Experimental results with temperature and salt density interfaces in single and double-stirred experiments show no significant differences in the mixing rate law; that is, for $Ri \geqslant 7$ the exponent $n = 1$ when the density difference is produced by temperature and $n = 1.5$ when produced by salinity. This suggests that molecular effects still dominate, since the temperature diffuses more rapidly than the salt, while u' and l' were varied little in his experiments. Turner [12] also proposed the Péclet number as a second dimensionless parameter in the mixing rate entrainment that takes into account the molecular diffusivity k of the stratifying component as well as the turbulence quantities:

$$Pe = \frac{u'l'}{k} \tag{7}$$

According to Crapper and Linden [1], the Péclet number was low in the temperature-stratified case ($Pe \leqslant 200$), and molecular diffusion influenced the interface structure across which all heat transport occurs by molecular diffusion. In the salt-stratified case, the Péclet number is high ($Pe \gg 200$) and thus nondiffusive processes control the entrainment. On the other hand, when $Ri \leqslant 7$, the exponent n was the same for both salt and heat stratification, suggesting that diffusion is less important in these cases.

Crapper and Linden [1] investigated the structure of the density interfaces over wide ranges of Péclet and Richardson numbers. Their results showed that the dimensionless interface thickness h/l' is independent of the Richardson number for high Péclet numbers and increased as Pe decreased, confirming Turner's results.

2. Experimental apparatus and methods

2.1. Experimental apparatus

Experiments were conducted in a rectangular tank (Fig. 1) of 270×270 mm inner cross section and 540 mm height, made of glass 10 mm thick. Three holes were drilled at the bottom of the tank; two of them allow filling and draining of the tank and the third allows positioning of the sampler pipe used to obtain vertical temperature and density profiles for the working fluid.

Two grids were machined in a square Plexiglass plate of thickness 10 mm and dimensions 250×250 mm. Each grid has 16 meshes of square geometry separated by bars of dimension $d = 10$ mm. The dimension of each mesh, defined as the distance between centres of two successive bars, is $M = 50$ mm, so the ratio $M/d = 5$. Each grid ends in a half-mesh, yielding 36% solidity. According to Shy et al. [13], this design satisfies the conditions suggested by Corrsin [14]: for solidity above 40% the wakes generated by grid oscillation may become unstable and therefore deviate from their original axes.

The grids are connected via two cylindrical rods of diameter 10 mm and square frame to an electric motor that transmits vertical oscillation to the grids by crank-connected rod systems. A radial groove machined in a wheel on the motor output shaft controls the stroke s of the grids. The tank is positioned on a support isolated from the motor to avoid transmitting vibration from motor to tank. The motor is connected to a variable-speed transmission by which its speed and thus oscillation frequency can be adjusted between zero and $f = 7$ Hz. In order to reduce the number of variables, a constant grid oscillation stroke $s = 10$ mm was used throughout and the oscillating grid frequency f was varied from 1 to 6 Hz.

The sampler pipe was made of two coaxial tubes of 800 mm length, 2 mm inside diameter and 3 mm outside diameter. The external tube assured the rigidity of the sampler, while the internal tube permits sampling of the working fluid in order to measure the vertical density profiles in the tank. The tube is also instrumented at its tip by an 80 μm thermocouple, allowing simultaneous measurement of the vertical temperature profile. The sampler pipe and tank were made watertight by a tightening device at the tank bottom. The sampler pipe could be moved vertically to take a fluid sample at different vertical positions through the tank. The system was coupled to a potentiometer that recorded the sampler pipe position during its displacement. The sampled fluid was then analyzed online by ANTON PAAR densimeter

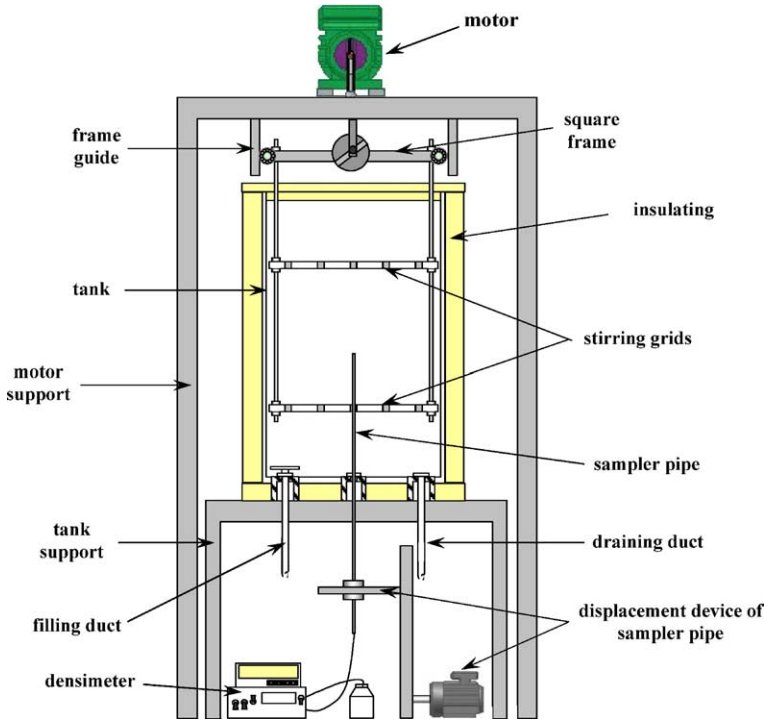

Fig. 1. Schematic diagram of the experimental apparatus.

equipped with a measuring cell whose volume is 0.7 cm^3 and concentration accuracy 10^{-5} g cm^{-3}.

Salinity stratification experiments were set up by first filling the tank with a homogeneous layer of fresh water at ambient temperature; then a salt-water layer of the desired concentration at ambient temperature was carefully injected through the bottom of the tank. For temperature stratification experiments, the tank was filled with a layer of hot fresh water and then filled from the bottom with a layer of cold fresh water. Both layers in each case were of equal depth and the grids were positioned in the middle of each homogeneous layer, 130 mm from the bottom and top of the tank. This procedure produced a thin salt or temperature interface between the two layers. Different initial salinity and temperature differences were used in the experiments. The salinity and heat fluxes were determined from the energy balance of either the lower or the upper layer.

2.2. Particle image velocimetry system

Since the quality of PIV measurements is highly affected by the optical deformation due to the variation of the refraction index inside the density interface, these measurements were conducted in a homogenous medium (water) where the position of the expected interface would be at the center of the enclosure at $z_g = 130$ mm.

The velocity field between the two grids was measured by the particle image velocimetry technique (PIV) diagrammed in Fig. 2. The flow was illuminated by a double-pulsed Nd:YAG laser (New Wave Minilase I-15) with minimal energy 100 mJ, which emits 532 nm green-wavelength light at pulse width 0.01 μs and repetition rate 10 Hz for each laser. The flow was seeded with hollow silver microspherical particles of density 1.49 and diameter 10–30 μm. The laser beams emitted by the two laser sources are combined through spherical and cylindrical lenses to obtain a thin light sheet to illuminate the seeding particles in the flow field. The light scattered by seeding particles provides a signal that is recorded on a digital CCD camera (Kodac Mega-plus ES1.0) of spatial resolution 1008×1018 pixels positioned perpendicular to the laser light sheet. The camera was operated in double-frame mode, and each frame was subdivided into a number of 32×32 pixel interrogation areas with 25% overlap.

The time delay between two successive pulses Δt was carefully set for each experiment in order to limit the number of incomplete particle pairs between two successive frames. To do this, we limited the displacement to one quarter of the interrogation area size L_{int}

$$\Delta t < \frac{L_{\text{int}}}{4U_{\max}} \tag{8}$$

where $U_{\max}$ is the flow velocity. The field of view was set as 130×130 mm so that it covered the interfacial region

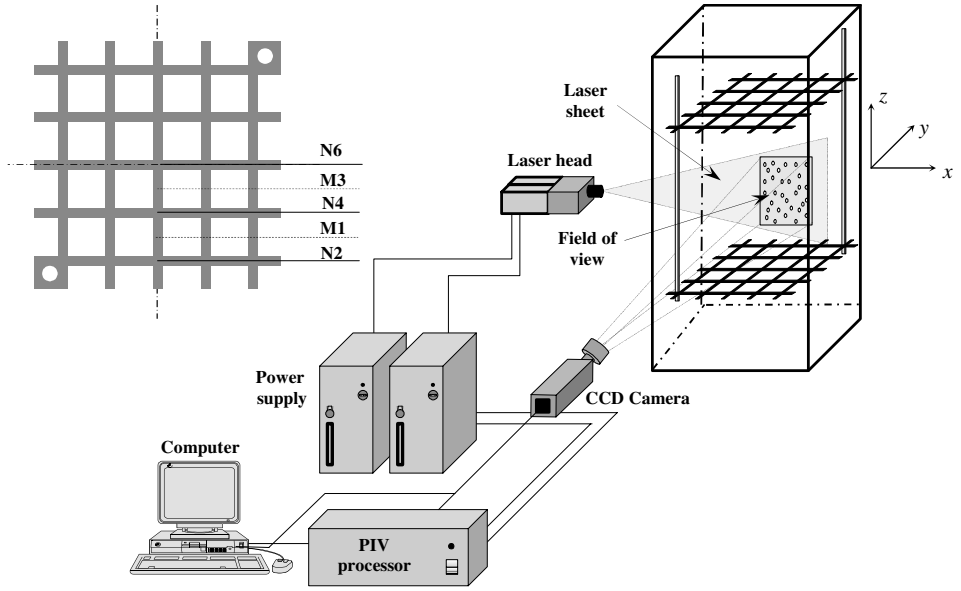

Fig. 2. Schematic diagram of PIV system and different viewing planes.

between the two grids, from the centre to the wall of the tank. A FFT-based cross-correlation algorithm process was used to analyse the frames and obtain the local displacement vector for each interrogation area. This processing yields a raw velocity vector map of the particles in the flow window studied.

Data acquisition and processing parameters were carefully optimized to provide high-quality results. Nevertheless, the raw vector maps contain a finite number of outliers (incorrect) vectors with different norms and orientations from surrounding valid vectors. The purpose of the validation method is to recognise, reject, and remove these outliers and possibly replace them with other vectors estimated from the surrounding measured vectors by a fast, reproducible automatic procedure using adaptive iterative interpolation. The Flow Manager software system was used for image recording, synchronization of lasers and CCD camera, and data processing.

2.3. PIV data analysis

Extensive PIV measurements were made to investigate the flow in the interfacial region between the two grids. The mean and fluctuating velocities were measured over five ($p = 5$) vertical planes, two at the centre of the grid mesh (M1 and M3) and three others at the grid bars (N2, N4, N6) (Fig. 2). The origin of z_g was taken as the grid mid-plane. The spatially rms velocities u' and v', respectively in the horizontal x and vertical z directions, were then estimated by averaging over the five measurement planes as follows. First, the spatially fluctuating velocities were calculated for $i = 41$ positions in the x-direction and $j = 42$ positions in the z-direction

$$u_p(x_i, z_j, n) = U_p(x_i, z_j, n) - \langle U_{j,p,n} \rangle_i \tag{9}$$

$$v_p(x_i, z_j, n) = V_p(x_i, z_j, n) - \langle V_{j,p,n} \rangle_i \tag{10}$$

where

$$\langle U_{j,p,n} \rangle_i = \frac{1}{41} \sum_{i=1}^{41} U_p(x_i, z_j, n) \tag{11}$$

$$\langle V_{j,p,n} \rangle_i = \frac{1}{41} \sum_{i=1}^{41} V_p(x_i, z_j, n) \tag{12}$$

where subscript N denotes the sampling number. The spatially rms horizontal and vertical velocities u' and v' are then calculated

$$u'(x_i, z_j) = \frac{1}{5} \sum_{p=1}^{5} \sqrt{\frac{1}{N} \sum_{n=1}^{N} u_p'^2(x_i, z_j, N)} \tag{13}$$

$$v'(x_i, z_j) = \frac{1}{5} \sum_{p=1}^{5} \sqrt{\frac{1}{N} \sum_{n=1}^{N} v_p'^2(x_i, z_j, N)} \tag{14}$$

To obtain the proper sampling number N for a good estimate of the spatial distribution of the mean velocities and turbulence statistics in the tank, we carried out a series of experiments with various sampling numbers N ranging from 1000 to 9000 samples. Selection of the appropriate sampling number is based on data convergence with the number of samples in PIV measurements [15].

Thus rms velocity component u' was calculated for different sampling numbers at the grids midway position $z_g = 130$ mm and for two frequencies $f = 3$ and 5 Hz. For $f = 3$ Hz, the convergence become quite stable beyond 5000 samples, while for $f = 5$ Hz convergence does not occur until $N = 7000$ samples. Therefore, all future results are based on an ensemble average of nearly $N = 10{,}000$ samples for each plane and frequency.

3. Characterization of grid-generated turbulence

3.1. Dependence of turbulent velocity on grid oscillation frequency

We explored the effect of the stirring frequency on the turbulence quantities over several z_g positions from the midplane of the grids. Fig. 3, plotting the horizontal turbulent velocity u' at different z_g positions, shows clearly that the horizontal turbulent velocity u' is linearly proportional to the grid oscillation frequency up to $f_c = 5$ Hz (the cutoff frequency [13]), but not for higher frequencies. Many authors have found this proportionality with different values of f_c; Shy et al. [13] found $f_c = 8$ Hz and explained this proportionality breakup by the generation of unwanted motions near the tank walls.

3.2. Velocity decay law

As indicated in the introduction, one must determine a spatial decay law for turbulence from both grids, defined as the energy sources. The results indicate that the normalized rms velocity in the x-direction decreases very rapidly away from the grid, following a power law well described by the typical equation (1) with a more quickly decreasing rate closer to the grid. For $s = 10$ mm and $M/d = 5$, the value of C_1 is 0.12 for frequencies $f \leqslant 5$ Hz and $1.2 < z_g/M < 2.6$. Ura et al. [11] noted that C_1 depends on the geometrical parameters of the grids if $s/M \leqslant 0.4$ and $z_g/M \leqslant 4$, which is the case in the present experiment.

In the various studies of grid turbulence, it is usually considered that the flow generated by the grids is symmetrical in a plan parallel to the grid in the range $z_g \in [M, 3M]$. This appears less obvious in a plan perpendicular to the grid [8]. Indeed, The measurements of vertical rms velocity scale showed that the ratio of vertical to horizontal rms velocities v'/u' is typically in the range $[1.1, 1.3]$ for $z_g < 2M$, highlighting a slight anisotropy in the flow in the plan perpendicular to the grids. On the other hand, in the range $2M < z_g < 2.6M$, the ratio v'/u' is close to 1 and the turbulent flow approaches an isotropic homogeneous flow, which is in good agreement with the literature [8,13,16,17].

3.3. Integral length scale

According to Kit et al. [18], the horizontal integral length scale based on the horizontal rms velocity is usually considered as the typical integral length scale in theoretical studies and this is valid for oscillating grid turbulence. The horizontal integral length scale is then calculated by integrating the spatial auto-correlation

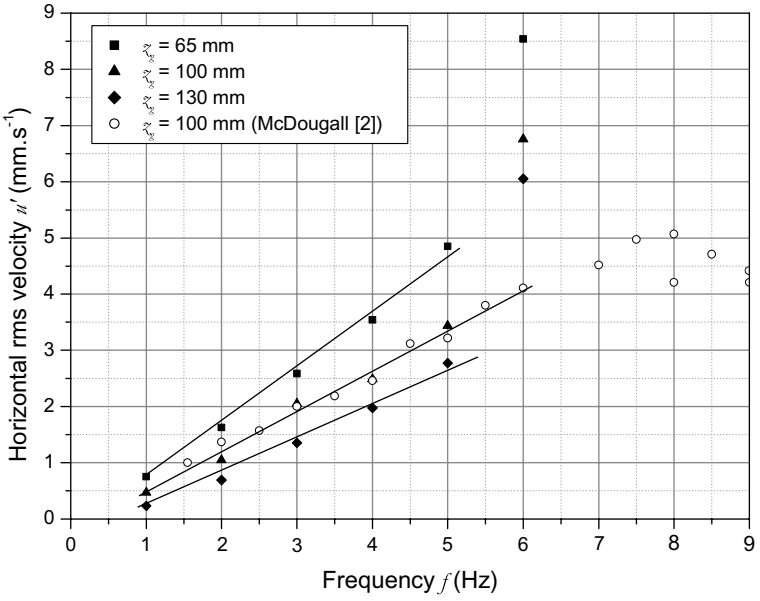

Fig. 3. Effect of grid oscillation frequency on horizontal rms velocity.

function, based on the horizontal rms velocity u', upto the first zero crossing

$$R(x,r) = \frac{\overline{u'(x)u'(x+r)}}{\overline{u'^2}} \tag{15}$$

Fig. 4 shows the variation of the horizontal integral length scale, between the two grids, as a function of the distance from the enclosure centre for frequencies ranging from 1 to 5 Hz. It can be seen that the integral length scale increases linearly with the distance from the grids z_g

$$l' = C_2 z_g \tag{16}$$

with the proportionality constant C_2 dependent on the experimental oscillation frequency. In the literature C_2 depends strongly on the geometry and the stroke of the grid [2,10]. However, according to Kit et al. [18], C_2 also depends on a variety of factors related to the experimental configuration. The integral length scale is inversely proportional to the grid oscillation velocity f_s and thus to the turbulence intensity [13] and cannot be a simple function of the stroke s, as assumed in Hopfinger and Linden [10]. The present measurements yield a value of C_2 ranging between $0.02 \leqslant C_2 \leqslant 0.05$ for $1 \leqslant f \leqslant 5$ Hz and $1.2 \leqslant z_g/M \leqslant 2.6$. The vertical integral length scale based on the vertical rms velocity was also calculated and compared to the horizontal integral length scale. The comparison shows that the ratio between the two quantities was also close to 1 in the same range of grid distance as for rms velocity components ($2M < z_g < 2.6M$). In the following stratified experiments, the frequency was fixed at 5 Hz and so the horizontal integral length scale and rms velocity, considered as the typical parameters of mixing, at the central position of the stratified interface ($z_g = 130$ mm) are constant ($l' = 12$ mm, $u' = 2.5$ mm s^{-1}). Thus the Richardson and the Peclet numbers depend respectively only on the density difference between the homogenous layers and the molecular diffusivity of the stratifying component.

4. Profile measurements

4.1. Methodology

In order to use the same methodology in the thermal and solute-stratified experiments, density profiles were deduced either from direct density measurements in an external device or from direct temperature measurements by an 80 μm thermocouple located at the tip of the sampler pipe (Fig. 1). Many salt solutions of known concentrations $0 \leqslant S \leqslant 15\%$ were realized and the calibration curve measured gives linear behavior of density versus concentration and temperature

$$\rho(T,S) = \rho_0(T_0,S_0)[1 - \alpha(T - T_0) + \beta(S - S_0)] \tag{17}$$

with $T_0 = 20$ °C, $\alpha = \alpha(T)$ and $\beta = 0.0072\%^{-1}$.

A deviation between the vertical position h and the corresponding fluid density or the corresponding temperature is induced either by the fluid transfer time from the sampling pipe opening to the densimeter measuring cell or by a small electronic time delay. This deviation is highlighted in Fig. 5 by an up–down traverse cycle of the sampler pipe. In order to avoid these discrepancies, all density profiles were measured from an up–down traverse of the sampler pipe. The height-density

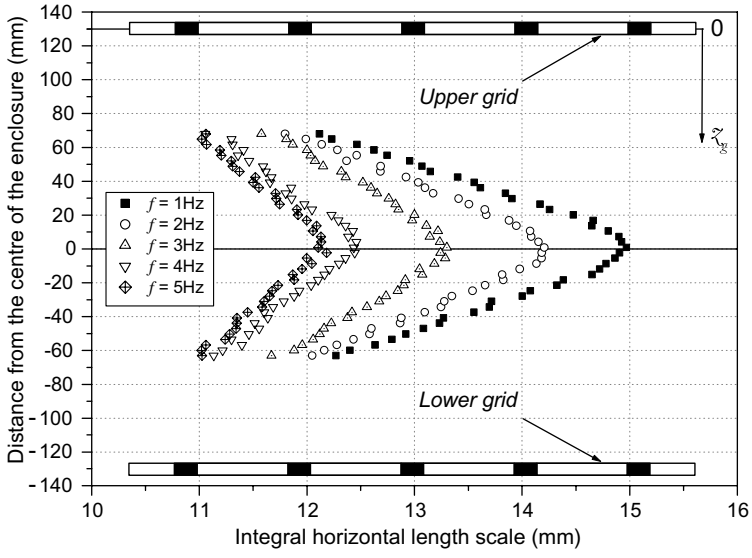

Fig. 4. Horizontal integral length scale for horizontal rms velocity component as a function of distance from interfacial region to grids.

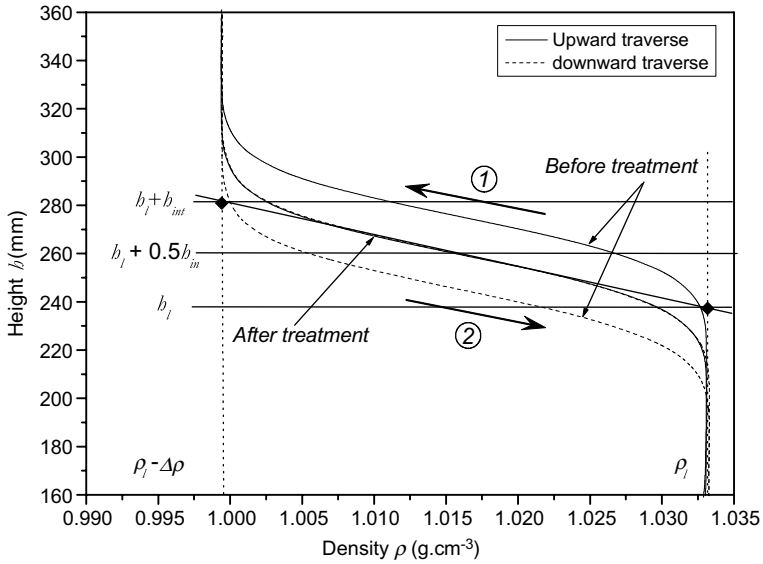

Fig. 5. Treatment of a density profile.

measurements were then corrected by subtracting the transfer time from both profiles. Fig. 5 shows clearly that, after this treatment, the profiles of one displacement cycle superimpose well one upon the other. The sampler pipe realizes measurement at 1 Hz and moves at 1.6 mm s^{-1}, requiring about 3 min for an up–down traverse cycle measurement on a height of 140 mm, including part of the lower and upper homogeneous layers and the complete interface, with no appreciable evolution of the stratification during the whole up–down measurement cycle.

The profiles in Fig. 5 permit the definition of several parameters such as the density step $\Delta\rho$ and the apparent interface thickness Δh by assuming a constant density gradient in the interfacial layer. The height of the lower layer is then h_l, the position of the interface is $h_l + h_{int}/2$ and the apparent density gradient is $\Delta\rho/h_{int}$. The term 'apparent' means that the profile does not take into account the temporal density fluctuations at each position due to such phenomena as internal waves and turbulent transport.

4.2. Time evolution

The quantity of fluid extracted (18 cm^3) during one displacement cycle of the sampler pipe was negligible for salt stratification and null for temperature stratification, so that at least 15 measurements can be achieved during one experiment without influencing stratification height. Fig. 6 shows vertical profiles for (a) salt and (b) temperature stratification characterized by two homogeneous layers separated by a thin interface. In Fig. 6a, the initial concentration step of salt is $\Delta S = 2.43\%$, which yields an initial density step $\Delta\rho = 20.76$ kg m^{-3}, larger than would be possible in the temperature-stratified case (Fig. 6b) where the initial temperature step was $\Delta T = 17$ °C. A fixed oscillation frequency $f = 5$ Hz was applied at time $t = 0$ and the density profiles were followed over time. Some diffusion of the interface occurs during filling the tank, but it was rapidly reduced by erosion of its upper and lower edges by the turbulent motions once the grids started to oscillate (Fig. 6). The turbulent flow in the lower and upper layers generated by the vertical oscillation of the two grids ensures good fluid homogeneity in the two mixed layers. Inside the interface, the vertical density profile remains roughly linear during all the experiments and the two limits of the interface are sharpened by the turbulence structures imposed by the grid. The interface is sharpened quasi-linearly on both sides of its upper and lower edges while its centre remains constant. The significant density gradient through the interface let us determine its position with relatively good precision.

In order to compare the two evolutions, the dimensionless density difference $\Delta\rho/\rho_0$ is represented as a function of time (Fig. 7). Two important points appear from this representation. First, for the same initial value of $\Delta\rho/\rho_0$ and for the same turbulence level, the time of total mixing is very different in the two cases: $t_{salt} > 5 \times 10^4$ s in the salt case and $t_{heat} = 8 \times 10^3$ s in the temperature case. Fig. 7a also shows that during the first moments of stirring in the salt-stratification case, the reduction in the density difference $\Delta\rho/\rho_0$ remains relatively linear with time however, it increases significantly at the end of the experiment i.e. the rate of $\Delta\rho/\rho_0$ reduction appears to increase with time. On the other hand, for

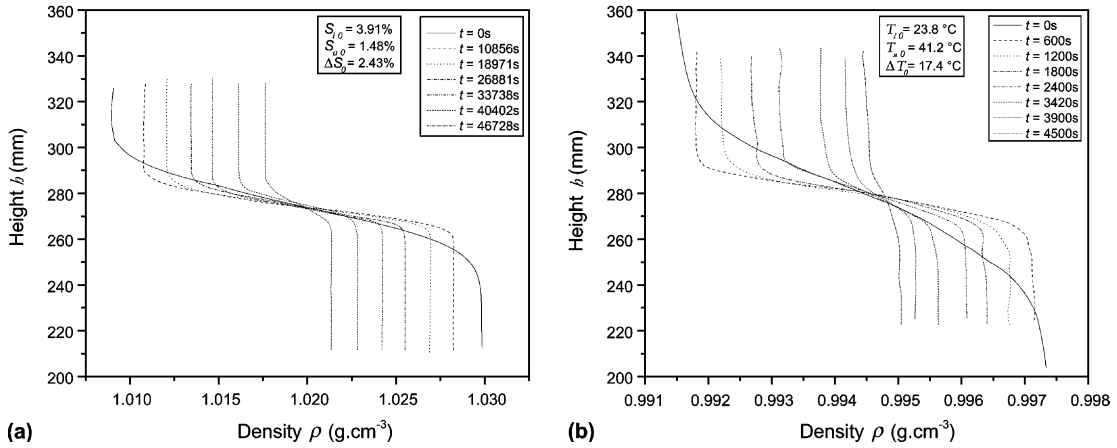

Fig. 6. Evolution of vertical density profile in time: (a) salt-stratified case and (b) temperature-stratified case.

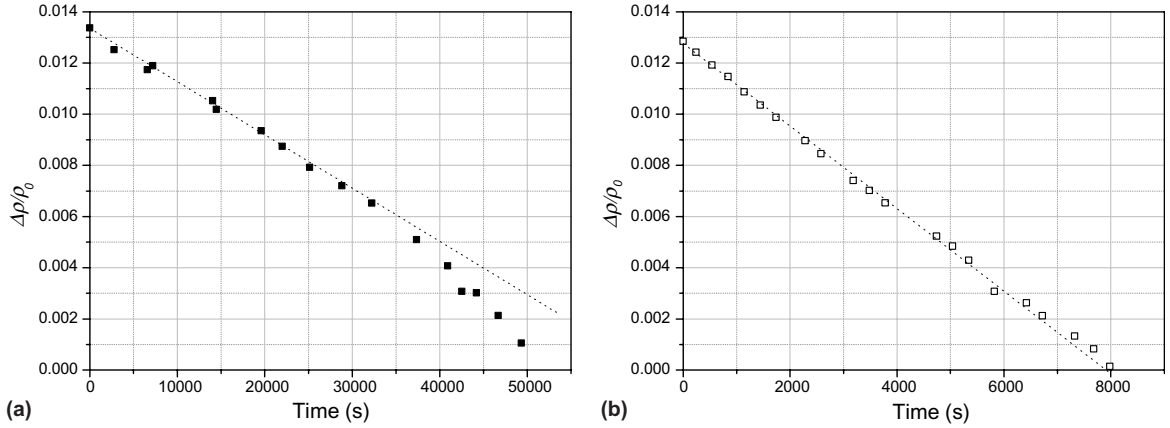

Fig. 7. Time evolution of density difference between two homogeneous layers for $f = 5$ Hz for salt (a) and for temperature (b) density interface.

temperature stratification, the rate of reduction of density difference seems constant during nearly all the experiment (Fig. 7b). Moreover, it should be noted that the common range of density difference in the two experiments let us compare the two buoyancy fluxes for the same flow regimes.

5. Flux measurements

5.1. Methodology

The heat flux F_T and the salt flux F_S across the density interface were computed from vertical temperature and salinity profiles over time in the two mixed layers. The balance between the two homogeneous layers leads to

For heat:

$$A_{\text{int}}\frac{\mathrm{d}}{\mathrm{d}t}\int_0^{h_l+h_{\text{int}}}\rho_l c_p T_l\,\mathrm{d}z = F_T A_{\text{int}} - (\varphi_{\text{losses}}A)_l \tag{18}$$

$$-A_{\text{int}}\frac{\mathrm{d}}{\mathrm{d}t}\int_{h_l+h_{\text{int}}}^{H}\rho_u c_p T_u\,\mathrm{d}z = F_T A_{\text{int}} + (\varphi_{\text{losses}}A)_u \tag{19}$$

where A_{int} is the interfacial area, ρ and T the density and the temperature of the layer, and c_p the constant-pressure specific heat. The thickness of the interface is not explicitly taken into account in calculating the heat and mass flux since the height of the two layers was measured from the central position of the interface. The heat losses φ_{losses} were estimated from a simple conduction model through insulation:

$$\varphi_{\text{losses}} = -\lambda_{\text{ins}}A_{\text{losses}}\frac{(T - T_a)}{e} \tag{20}$$

where λ_{ins} and e are the insulation thermal conductivity and thickness respectively, T_a is the ambient temperature and A_{losses} is the surface insulation.

For salt:

$$F_S = \frac{d}{dt}\int_0^{h_1+\frac{h_{int}}{2}} \rho_0 S_l \, dz = \frac{d}{dt}\int_{h_1+\frac{h_{int}}{2}}^{H} \rho_0 S_u \, dz \qquad (21)$$

where S is the salt concentration.

5.2. Experimental measurements

In order to compare directly the two fluxes of heat and mass, we plot on Fig. 8 the evolution of the heat $\alpha F_T/\rho_0 c_p$ and salt $\beta F_S/\rho_0$ buoyancy fluxes, defined as the potential energy changes due to the transfer of heat and salt across the density interface [6], according to the relative density difference between the two mixed layers. The two fluxes present two different behaviors. For the salt stratification, the salt buoyancy flux increases with decreasing density difference between the two mixed layers while the heat buoyancy flux decreases. Thus an interpretation of the flux as proportional to the property difference is possible for the heat interface with a quasi-constant transfer coefficient. On the other hand, for the salt interface the transfer coefficient should be highly dependent on the stability of the interface with probably a change in the transport regime. For the same density difference and the same turbulence level, the buoyancy flux is larger in the heat case, indicating a strong effect of molecular diffusivity on the flux across the interface.

5.3. Entrainment

Since the turbulence level is balanced on both sides of the interface, the entrainment of interfacial fluid towards the lower layer is equal to that towards the upper layer. Then the position of the interface in the middle of the tank remains unchanged. In this case, the entrainment can be deduced from the property flux [12].

From a phenomenological argument, one can postulate that the flux entering a homogeneous layer is incorporated through the entrainment mechanism. Then, defining the entrainment rate u_e by the rate of volume incorporation into a homogeneous layer, the corresponding flux is

$$\phi_e = u_e \Delta\rho A_{int} \qquad (22)$$

Fig. 9 plots the mixing rate $E = u_e/u'$ as a function of the Richardson number Ri when the density difference is produced by temperature as well as by salt. The entrainment velocity u_e was deduced from the flux measurement using Eqs. (5) and (6), and the grid stirring frequency was fixed at $f = 5$ Hz. The variation in the Richardson number is then due only to the reduction in the density step between the two mixed layers. The result are in good agreement with those of Turner [12]; that is, on the one hand, the rate of mixing increases with decreasing Ri and is higher in the temperature case than in the

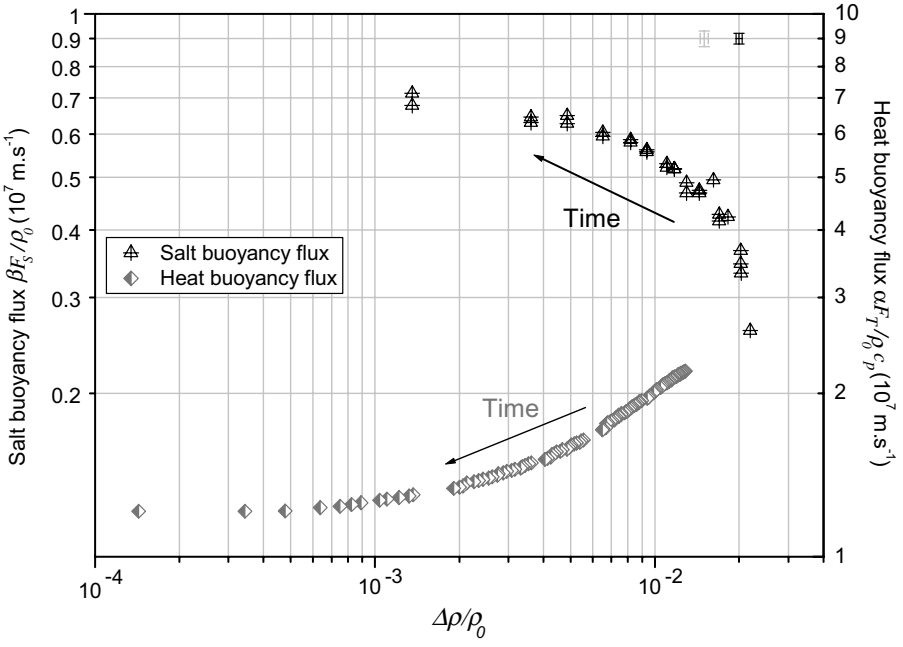

Fig. 8. Salt and heat buoyancy flux as a function of dimensionless density difference.

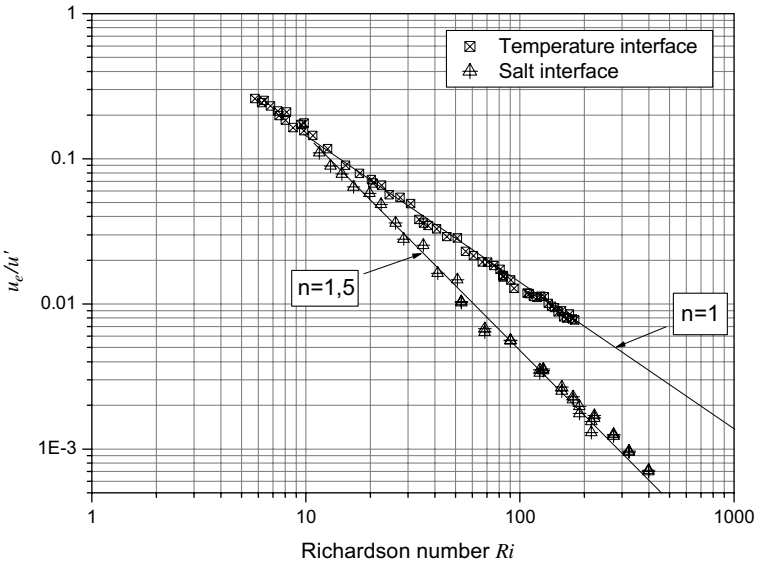

Fig. 9. Mixing rate as a function of Richardson number for temperature- and salt-density interface.

salt case over a wide range of Ri ($Ri > 10$). On the other hand, the mixing rate for the temperature-density interface is best represented by a line of slope -1 and for the salt-density interface by a line of slope -1.5. For low Richardson number ($Ri < 10$), the mixing rate is the same for both cases.

Two important aspects emerge from these representations: the buoyancy and the molecular effects. The slope of the two lines in Fig. 9 shows that the mixing rates should be attributed not to the viscosity difference, since it does not vary greatly in the two experiments, but to the large difference in molecular diffusivity between the two diffusing components, heat and salt. A fluid element entrained from the temperature interface diffuses more rapidly than that entrained from the salt interface, which returns to the interface by buoyancy effects to be dissipated mainly in wavelike motion [12]. In the present temperature experiments the Peclet number $Pe = u'l'/k$ was around $Pe \approx 200$ and in the salt case it was above 2×10^4. Then the mixing efficiency of turbulent entrainment differs drastically in the two cases.

When the Richardson number decreases, the mixing rate for the salt component increases, approaching and then attaining that of the temperature component. Fig. 10 clarifies this evolution in terms of the potential energy of the stratification, i.e., the density difference $\Delta\rho$ between the two mixed layers. The larger $\Delta\rho$, the stronger the stratification, so that the energy required to destabilize it must be higher. The turbulent structures are in this case severely damped near the salt interface, and entrainment of heavy fluid events from the interface to the mixed layer is rare and intermittent. The salt mixing rate is then weak. When the density difference $\Delta\rho$ across the interface decreases, the interface becomes more vulnerable to the turbulent structures, which are now more or less able to penetrate it and to entrain lighter fluid from it to mix more efficiently with the mixed layer and to increase the mixing rate. Thus transport is dominated by mechanical mixing near the interface. At small values of Ri ($Ri < 10$), molecular effects become less important compared to the effect of agitation and the two curves approach the same value. These remarks are supported by simple visual observations of the evolution of the stratification: we see very sharp and stable edges of the interface during the first moments of agitation and an agitated interface at the end of the experiment, with more frequent fluid entrainment events.

6. Discussion

6.1. Comparison with double-diffusive convection

Heat and salinity fluxes across a stratified interface in *grid turbulence* have not so far been compared with natural convection. The question arises of the role of turbulence as the transfer vector and its difference from natural convection. In order to normalize the heat and salinity fluxes we define, as in Turner [19], the notion of the *reference heat flux* as the flux that would have been transferred were the liquid stratified interface replaced by a horizontal *perfectly* conducting solid plate. The best correlation with this *reference* is obtained in turbulent natural convection over a heated flat plate, for which the flow parameter, the Rayleigh number, was replaced by a combination of the Reynolds and

Prandtl numbers in order to obtain the same level of velocity fluctuations. We thus use the following expression for the Nusselt number [20]:

$$Nu_{TP} = C_T (Re_L^2 Pr)^{1/3} \tag{23}$$

where Nu_{TP} is the dimensionless heat flux through the solid plate, Re_L is the Reynolds number based on the characteristic length of the solid plate defined as $L \equiv A_S/P$ (where A_S and P are the plate surface area and perimeter respectively), and Pr is the Prandtl number. The plate heat flux is then defined as

$$F_{TP} = C_T \rho_0 c_p k_T \frac{\Delta T}{L} (Re_L^2 Pr)^{1/3} \tag{24}$$

k_T being the thermal conductivity and c_p the constant-pressure specific heat. By the heat-mass analogy, we also define a mass transfer flux through a horizontal solid plate:

$$F_{SP} = C_S k_S \rho_0 \frac{\Delta S}{L} (Re_L^2 Sc)^{1/3} \tag{25}$$

where Sc is the Schmidt number and k_S is the salt diffusivity; C_T and C_S are constant empirical coefficients to be obtained from experiment.

6.2. Experimental comparison

Figs. 10 and 11 plot the dimensionless heat F_T/F_{TP} and mass flux F_S/F_{SP} as a function of Richardson number. For comparison, Fig. 10 also superposes the evolution of the dimensionless heat and salt fluxes in the *double-diffusive convection* obtained by Turner [19] for convective heat-salt system and Gorieu [21] for a convective heat-freon system. In fact, one can consider the Richardson number as analogous to the interfacial stability number (ratio) since they are both ratios of stabilizing to destabilizing forces. The interfacial stability ratio defined by Turner as $R_\rho = \beta\Delta S/\alpha\Delta T$ is also shown in Fig. 10, where β and α are the mass and thermal expansion coefficients, respectively; this ratio was obtained from an analogy between a stirred and non-stirred system considering a convection characteristic velocity defined as $U_C = \sqrt{g\alpha\Delta T L_C}$, where L_C is a convective characteristic length scale. We redefine the interfacial stability ratio as

$$R_\rho = \frac{\beta}{\alpha}\frac{\Delta S}{\Delta T} = \frac{\beta \Delta S}{U_C^2/gL_C} \tag{26}$$

where L_C is the layer depth h and $U_C = f_s$ the characteristic velocity of the grid.

The interfacial heat flux in Fig. 10 for high Richardson numbers ($Ri > 120$) goes below the flux value across a solid horizontal plate. This is explained by the fact that at the beginning of the experiment the density difference is high and thus the potential energy of the stratification is significant, making the interface stable. The kinetic energy contained in the turbulent structures generated by stirring is still insufficient to deform and entrain fluid from the interface, so that the interface has a finite thickness with internal diffusion. Nevertheless, since the fluid diffusivity is not *infinite*, as hypothesized in the solid

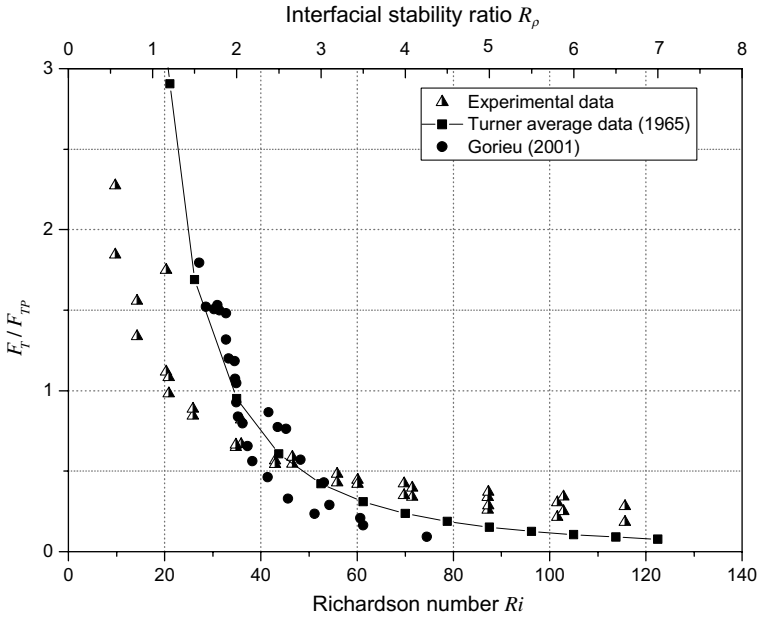

Fig. 10. Dimensionless heat flux versus Richardson number.

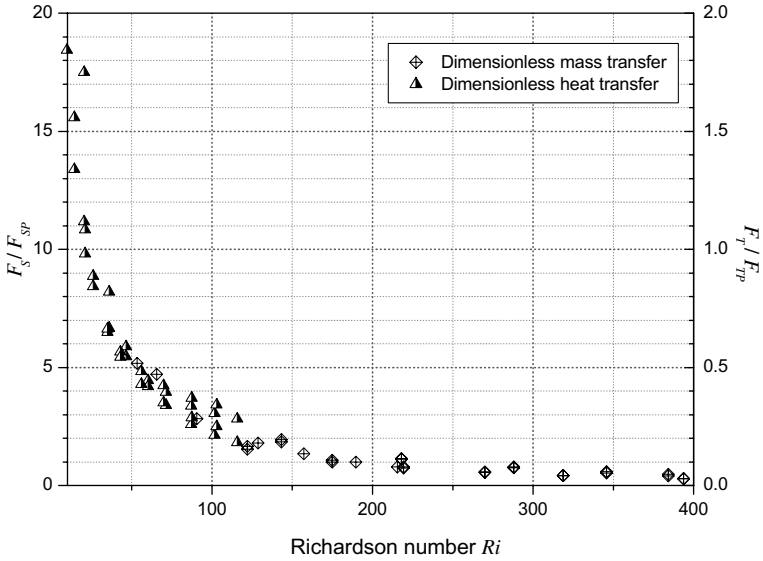

Fig. 11. Heat and salinity transfer fluxes across density interface as a function of Richardson number.

flat-plate *reference flux*, the measured nondimensional flux is less than one.

As Ri decreases, the potential energy of the stratification decreases and the interface becomes less stable. The effect of turbulence intensity increases and deforms the interface, whose thickness becomes very thin. As the layer thickness decreases, so does the diffusion flux inside the interface. This increase may also be partially associated with the fact that the *thin* interface behaves increasingly like a free surface, so that horizontal motion is more weakly constrained and supports waves that can break and increase the effective surface and hence mixing.

For very low values of $Ri < 10$ the dimensionless heat flux becomes significant, reaching nearly ten times its value when $Ri > 120$. The heat flux is then dominated by direct mechanical mixing between the two homogeneous layers, with no measurable interfacial layer.

Almost the same observations can be made for the salt stratification. The salt flux increases exponentially with decreasing Ri, indicating that at the beginning of the experiment entrainment events are rare, so the dimensionless salt flux is weak. It reaches a value ten times larger when $Ri = 50$, which confirms again that mechanical mixing becomes the dominant transfer process. This is in good agreement with the results of Crapper [22] for weak agitation, equivalent to our case when stratification is strong. Nevertheless, in the absence of a transport model across the interface, these results must be rescaled by a factor (C_T and C_S), since in calculating the dimensionless heat and salt transfer an empirical correlation was used and an analogy between heat and salt fluxes was assumed.

7. Conclusions

This study reports on controlled laboratory experiments that permit measurement of both turbulent fields in a homogenous fluid generated by vertically oscillating grid in the range $1 < f < 5$ Hz and heat and mass fluxes across a density-stratified interface for a large range of Richardson numbers (10–400) for two components of two very different molecular diffusivities, namely temperature and salt. We have expressed the turbulence generated by grid oscillation in terms of turbulent horizontal velocity u' and length scale l'. In the range of the oscillation frequency studied, the results are in good agreement with laboratory measurements [13].

The measured heat and salt buoyancy fluxes in stratified grid turbulence showed two different evolutions, both similar to that in a double-diffusive convection system. This similarity was highlighted by measurement of the entrainment rate across the density interface, which showed that both heat and salt fluxes depend on the Peclet number (not on molecular diffusivity) for high Richardson number. For low Richardson numbers, the entrainment rates for heat and salt approach the same value, suggesting that the molecular diffusion mechanism has no less effect on the transport process than turbulent mixing. In this regime, the interface is much weaker and distorted, leading to physical contact between turbulent eddies from both upper and lower layers and thus increasing the flux across the stratified interface layer. However, it should be noted that the interface thickness cannot be determined from measured vertical density profiles of salt and temperature, as has been done previously, since this method overestimates the

layer thickness compared with the real thickness (measured, for instance, by LIF visualizations), and therefore underestimates the diffusive flux across the interface, especially in the high-Richardson-number regime. Also, measurements of dimensionless heat and mass fluxes showed remarkably a similar evolution to that reported by Turner in *double-diffusive convection* [19], represented by a power law such as $F_{(S,T)}/F_{(S,T)P} = C_{(S,T)}Ri^{-1/n}$. We found $C_T \approx 1$ in the temperature case and $C_S \approx 10$ for salt. The value of C_S was obtained by adjusting the dimensionless mass flow to that of heat, indicating that the flat-plate flux formula overestimates the dimensionless mass flux, since the latter must be smaller than that of heat.

Finally, the above remarks suggest that a transfer model is needed that either takes into account the influence of the molecular diffusivity on the entrainment through the Peclet number ϕ_e (Ri, Pe) or is based on a turbulent diffusion coefficient $(k_\rho(Ri, k))$ across the interface that can be estimated from flow measurements inside the interface [23].

Acknowledgement

The financial support provided by ADEME (Agence de l'Environnement et de la Maîtrise de l'Energie) for this work is highly acknowledged. YZ is indepted to Professor J.S. Turner for helpful comments on parts of this work.

References

[1] P.F. Crapper, P.F. Linden, The structure of turbulent density interface, J. Fluid Mech. 65 (1) (1974) 45–63.
[2] S.M. Thompson, J.S. Turner, Mixing across an interface due to turbulence generated by an oscillating grid, J. Fluid Mech. 67 (2) (1975) 349–368.
[3] R.I. Nokes, On the entrainment rate across a density interface, J. Fluid Mech. 188 (1988) 185–204.
[4] M.J.A.M. Perera, H.J.S. Fernando, D.L. Boyer, Turbulent mixing at an inversion layer, J. Fluid Mech. 267 (1994) 275–298.
[5] H.E. Huppert, J.S. Turner, Double-diffusive convection, J. Fluid Mech. 106 (1981) 299–329.
[6] J.S. Turner, Buoyancy Effects in Fluid, Cambridge University Press, 1998.
[7] H. Rouse, J. Dodu, Turbulent diffusion across a density discontinuity, Houille Blanche 10 (1955) 530–532.
[8] T.J. McDougall, Measurements of turbulence in a zero-mean-shear layer, J. Fluid Mech. 94 (1979) 409–431.
[9] J.F. Atkinson, Interfacial fluxes at a grid-stirred diffusive interface, International Journal of Heat and Mass Transfer. 37 (14) (1994) 2089–2099.
[10] E.J. Hopfinger, J.A. Toly, Spatially decaying turbulence and its relation to mixing across a density interface, J. Fluid Mech. 78 (1976) 155–175.
[11] M. Ura, T. Tsubaki, N. Matsunaga, A turbulence-based expression for the entrainment coefficient for two-layered stratified flows, J. Hydrosci. Hydraul. Eng. JSCE 5 (1) (1987) 27–37.
[12] J.S. Turner, The behaviour of stable salinity gradient heated from below, J. Fluid Mech. 33 (1968) 183–200.
[13] S.S. Shy, C.Y. Tang, S.Y. Fann, A nearly isotropic turbulence generated by a pair of vibrating grids, Experimental Thermal and Fluid Science. 14 (1997) 251–262.
[14] S. Corrsin, Turbulence: experimental methodsHandbuch Der Physik, Stromungs Mechanik. II, vol. 8, Springer-Verlag, Berlin, 1963, pp. 524–587.
[15] S.Y. Son, K.D. Kihm, J.C. Han, PIV flow measurements for heat transfer characterization in two pass-square channels with smooth and 90° ribbed walls, Int. J. Heat Mass Transfer 45 (24) (2002) 4809–4822.
[16] I.P. De Silva, H.J.S. Fernando, Oscillating grids as a source of nearly isotropic turbulence, Phy. Fluids 6 (7) (1994) 2455–2464.
[17] P. Chassaing, Turbulence en mécanique des fluides, Analyse du phénomène en vue de sa modélisation à l'usage de l'ingénieur. Editions Cépadués, Coll. Polytech, Toulouse, 2000.
[18] E.L.G. Kit, E.J. Strang, H.J.S. Fernando, Measurement of turbulence near shear-free density interfaces, J. Fluid Mech. 334 (1997) 293–314.
[19] J.S. Turner, The coupled turbulent transport of salt and heat across a sharp density interface, Int. J. Heat Mass Transfer 8 (1965) 759–767.
[20] F.P. Incorpera, D.P. Dewitt, Introduction to Heat Transfer, third ed., John Wiley & Sons Inc., 1996.
[21] O. Gorieu, P. Dupont, Y. Zellouf, H. Peerhossaini, Mesures expérimentales des flux de chaleur et de masse à travers une interface de densité, Congrès français de Thermique SFT, 2001, pp. 29–31.
[22] P.F. Crapper, Fluxes of heat and salt across a diffusive interface in the presence of grid-generated turbulence, Int. J. Heat Mass Transfer 19 (1976) 1371–1378.
[23] G.N. Ivey, K.B. Winters, I.P.D. De Silva, Turbulent mixing in a sloping benthic boundary layer energized by internal waves, J. Fluid Mech. 418 (2000) 59–76.